

Dynamic Swirl Distortion Characteristics in S-shaped Diffusers using UCNS3D and Time-resolved Stereo PIV Methods

Tommaso Piovesan¹, Matteo Migliorini², Pavlos K Zachos³ and Panagiotis Tsoutsanis⁴

School of Aerospace Transport and Manufacturing Cranfield University, Bedfordshire, MK43 0AL, UK

Embedded propulsion systems are key enablers of future aircraft configurations with expected benefits in reduced environmental impact and enhanced performance. Such propulsion systems are typically integrated with convoluted, complex air induction systems whose dynamic distortion characteristics previously found detrimental to the engine's stability. Therefore, predictive capability for these complex flows is critical for the design of closely coupled engine – intake architectures. A new High-Order Delayed Detached Eddy Simulation (HODDES) is applied in this work to predict dynamic flow distortion within an S-shaped subsonic diffuser. The aim is to assess the ability of a new solver to predict unsteady and extreme distortion events. The HODDES results have been validated with Time-Resolved Stereo PIV (TR-PIV) data. The analysis shows that the HODDES captures the key mean and unsteady flow characteristics, the spectral content and unsteady distortion descriptor behavior across the Aerodynamic Interface Plane (AIP). Although the predicted mean velocity levels, flow field unsteadiness and range of predicted velocities are notably higher than the ones observed at the experiment by at least 40%, it is suggested that this is an artifact of a discrepancy between the axial planes where the CFD and test data were analyzed. The findings of the work suggest that the HODDES is broadly capturing the dynamic flow fields and with some further effort towards the calibration of its RANS models can be further used to study the integration of closely coupled fan system downstream of air induction systems.

¹ Doctoral researcher, Centre for Propulsion and Thermal Power Engineering.

² Senior Research Fellow, Centre for Propulsion and Thermal Power Engineering.

³ Reader in Propulsion Aerodynamics, Centre for Propulsion and Thermal Power Engineering, AIAA Member.

⁴ Reader in Computational Fluid Dynamics, Centre for Computational Engineering Sciences.

Nomenclature

D	=	Cross-sectional diameter of the S-duct, mm
f	=	Frequency, Hz
h	=	Centerline offset of the S-duct, mm
$j\text{-PDF}$	=	joint-Probability Density Function
L	=	Axial length of the S-duct, mm
M	=	Mach number
PS	=	Power Spectrum
px	=	Pixel
Re_D	=	Reynolds number relative to a diameter
SD	=	Swirl Directivity
SI	=	Swirl Intensity, deg
SP	=	Swirl Pairs
St	=	Strouhal number, $fD_{AIP}/\langle\bar{w}\rangle_{AIP}$
TKE	=	Turbulent Kinetic Energy, J/kg
u, v, w	=	Cartesian velocity components, m/s
α	=	Swirl angle, deg

Abbreviations

AIP	=	Aerodynamic Interface Plane
$DEHS$	=	di-Ethyl-Hexyl Sebacate
$(HO)DDES$	=	(High-Order) Delayed Detached Eddy Simulations
LES	=	Large Eddy Simulations
$MIDAS$	=	Modern Intake Distortion Analysis System
$MUSCL$	=	Monotonic Upstream-centered Scheme for Conservation Laws
POD	=	Proper Orthogonal Decomposition
$RANS$	=	Reynolds Averaged Navier-Stokes
$TR\text{-}PIV$	=	Time-resolved Particle Image Velocimetry

Subscripts

in	=	Inlet plane of S-duct
out	=	Outlet plane of S-duct
ref	=	Reference plane

Operators

$\langle \cdot \rangle$	=	Time-average
$\bar{\cdot}$	=	Area-average
σ	=	Standard deviation
$Var(\cdot)$	=	Variance

I. Introduction

Advanced airframe configurations with complex air induction systems are anticipated to be central points in the installation of future propulsion systems to meet environmental and performance targets [1] [2]. These configurations are thought to enable reductions in drag and weight which will reflect in the overall fuel burn and emissions signature of the system. However, the complex intakes that deliver the free-stream flow to the aero engine promote high levels of unsteady flow distortions ([3] [4] [5]). The characteristics of these unsteady flows, and consequently the unsteady distortions at the AIP, may vary across the operational range of the system and may yield a penalty in the stability margin of the engine that can be detrimental for its operability ([6]-[11]). Typical results from pressure measurements within an S-duct configuration were previously presented by Wellborn et al. in [12]. In this work the flow within a diffusing S-duct intake whose vertical offset was $h/L=0.27$, area ratio between the exit and the inlet of 1.52 and non-dimensional length of $L/D_{in}=5.0$ was characterized experimentally. These results showed a large total pressure deficit located at the lower part of AIP along with the presence of two counter-rotating swirling flow patterns, symmetrically positioned in relation to the vertical axis. More recent studies by Delot et al. ([13] [14] [15]) and Garnier [16] showed unsteady total pressure measurements within two S-shape diffusers with vertical offsets of $h/L=0.27$ and $h/L=0.49$ respectively aligned with the work of Wellborn et al. [12]. These studies demonstrated that Mach and Reynolds number variations at the inlet of the intake have a weak, second order impact on the dynamic flow characteristics. The work by Giuliani and Chen [17] on a boundary layer ingesting semi-embedded fan and intake configuration, demonstrated that non-uniformities at the total pressure profile at the inlet of the intake are strongly linked to the unsteady distortion characteristics at the AIP and to the fan stall inception mechanism. In this work, the necessity of characterizing the unsteady distortion signature of convoluted intakes across a range of operating conditions is strongly emphasized. These conditions may be represented by variations of the total pressure or velocity profile upstream of the intake and a sub-set of these was previously investigated in terms of their impact on unsteady distortions by McLelland et al. [18] and Migliorini et al. [19]. Both these studies indicated that there is a notable discrepancy between the unsteady distortion aspects of a baseline case with a nominal inlet flow profile and cases where the inlet flow pressure profile would follow a non-uniform distribution.

Historically, in large scale development programmes, flow distortion has been characterized by means of pressure probe rakes at the Aerodynamic Interface Plane (AIP) to capture the pressure variations across the plane [6]. In most of the cases, low number and low temporal bandwidth pressure measurements are only acquired, sometimes complimented by a small number of unsteady sensors which were found to provide only a poor indication of the flow unsteadiness within the domain [6]. Nevertheless, the significance of the dynamic component of the flow distortion has been repeatedly highlighted in past studies as a key aspect for the successful integration between a propulsion system and a complex intake [11]. To address the need for more representative unsteady measurements, a more advanced measurement method was introduced by Zachos et al. [3] and Gil-Prieto et al. [20]. These studies demonstrated the use of stereoscopic, particle image velocimetry (S-PIV) for velocity field flow measurements in a synchronous way across the entire AIP plane with notably higher spatial resolution than the previous studies. In addition, Gil-Prieto et al. [4] also demonstrated the use of time-resolved, stereoscopic particle image velocimetry (TR-PIV) for AIP velocity measurements which enabled the flow analysis in the temporal domain to characterize the dynamic distortions.

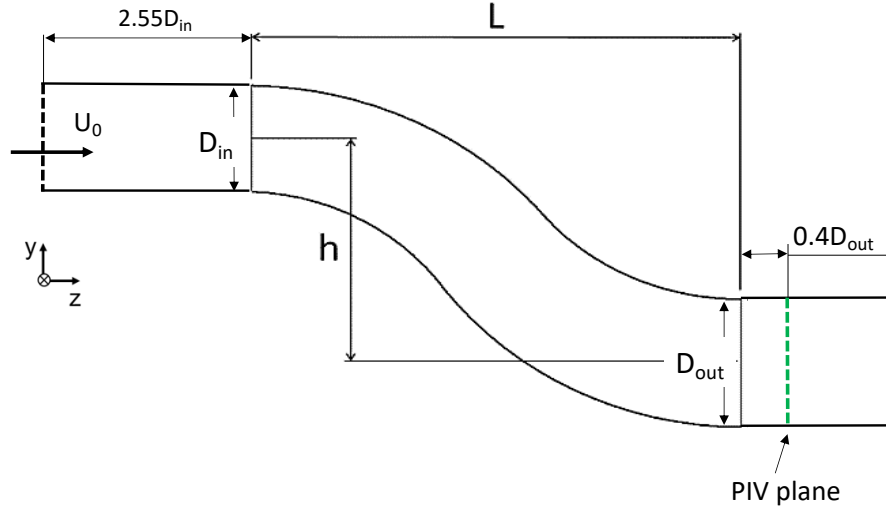
In parallel to the development of advanced experimental methods for flow measurements within S-duct intakes, a number of computational studies were also undertaken. Delot et al. [13] showed Large Eddy Simulation (LES) results which successfully predicted the experimentally measured levels of flow unsteadiness albeit the high computational cost. Further work by Delot et al. [14] reported several variations of Reynolds Averaged Navier-Stokes (RANS) computational studies for an S-duct diffuser showing that two-equation turbulence models tend to match test data better than simpler variations although no unsteady simulations were conducted as part of this work hence no comparisons on the unsteady flow statistics could be made. Addressing this issue, hybrid methods that combine LES and RANS modelling were also previously shown as a compromise between computational cost and prediction accuracy to perform unsteady simulations. MacManus et al. [21] used Delayed Detached Eddy Simulations (DDES) for unsteady flow predictions within the S-shaped ducts previously studied by Delot et al. [13] [14] and Garnier [16]. The DDES results were aligned with the outcomes from Delot et al. [13] [14] and Garnier [16] in terms of predicting the frequencies of the main unsteady flow perturbations at the AIP flow field. Further numerical simulations were shown by Gil-Prieto et al. [5] for the high offset S-shaped diffuser configuration ($h/L=0.49$) also used by Zachos et al. at $Ma_{ref}=0.27$ [3]. In this study standard DDES methods were validated against PIV data. As part of this work, Proper Orthogonal Decomposition (POD) was used to assess the coherent structures within the underpinning flow field. Four main modes were identified as the most energetic; two vertical and two laterally oscillating ones. The latter were

correlated with a swirl switching mechanism which was responsible for the alteration of the flow between two conditions that were dominated by clockwise and a counter-clockwise Dean vortex respectively similar to these shown by Kalpakli-Vester in non-diffusing, 90° bends [22] [23]. The unsteady analysis by Gil-Prieto et al. [5] also demonstrated that the lateral switching mechanism of the flow had a dominant frequency of $St=0.5$ which was associated with the unsteadiness originally developed at the separation zone located within the S-duct. The main vertical mode was found predominantly at a frequency of $St=1.06$ and was promoted by spanwise vortices which were shed in the shear layer from the main separation region. These observations were further confirmed by the unsteady analysis of TR-PIV data by Gil-Prieto et al. [4] for the S-duct with $h/L=0.49$ at $M_{ref}=0.6$. This confirms that the unsteady characteristics of the flows within these intakes remain predominately unchanged for a range of subsonic Mach numbers at the inlet. Furthermore, the study by Gil-Prieto et al. [5] [20] demonstrated that for the S-shaped diffuser with $h/L=0.49$ at $M_{ref}=0.6$ the unsteady behavior of key swirl distortion descriptors is primarily dominated by frequencies linked to the switching modes revealed by the POD analysis. In particular, dominant frequencies of around $St=0.5$ were detected in the unsteady signals of both the Swirl directivity (SD) and Swirl Intensity (SI) descriptors across a range of radial positions over the measurement plane. These frequencies were found to be within the range of the critical frequencies to which a typical aero-engine fan is likely to respond therefore they may have an adverse impact on the propulsion system [10].

In this context, the current work shows the application of a High-Order DDES (HODDES) method to capture the key dynamic attributes of the complex flows within convoluted engine diffusers and validate the calculations against experimental data obtained via TR-PIV. This HODDES method is based on the implementation of the high-order finite-volume UCNS3D software [24] where a 3rd-order Monotone Upstream centered Scheme for Conservation Laws (MUSCL) is used, where it has previously demonstrated an improved capability to resolve fine features of the flow free from spurious-oscillations for a wide-range of compressible flow problems while exhibiting substantially better parallel efficiency compared to the standard 2nd-order schemes [24]. To validate the HODDES method, the predicted flow characteristics are compared against TR-PIV data for this particular S-shaped diffuser. The flow statistics at the AIP were evaluated and spectral analysis of the dynamic AIP swirl angle was carried out. The dynamic distortion characteristics of the flow are investigated via unsteady swirl distortion descriptor joint probability function maps.

II. Experimental Setup and Numerical Methods

The S-duct geometry used in this study is the geometry previously tested by Zachos et al. [3]. The inlet and outlet cross sections are circular, with an area ratio between inlet and outlet planes of $A_{out}/A_{in} = 1.52$. The axial length was $L/D_{in} = 4.95$ while the vertical offset was $h/L=0.49$. The Aerodynamic Interface Plane (AIP) where the PIV measurements were conducted had a diameter of $D_{out} = 150$ mm (see Figure 1) and was located approximately $0.4D_{out}$ downstream of the intake's exit plane. The results included in this investigation correspond to an inlet reference Mach number $M_{ref}=0.27$ ($Re_D = 5.9e+05$). This was measured at a reference plane positioned $1.45D_{in}$ upstream of diffuser's inlet. The thickness of the boundary layer at this plane was $\delta/D_{in}=0.04$. The operating Mach number uncertainty was about 0.27 ± 0.001 and considered the calibration uncertainty and the accuracy and resolution of the pressure transducers [4].



Parameter	High offset S-duct
A_{out}/A_{in}	1.52
L/D_{in}	4.95
h/L	0.49
D_{out} [mm]	150.0

Figure 1 Schematic of the convoluted S-shaped diffuser and geometry specification.

Time resolved stereo Particle Image Velocimetry (TR-PIV) was applied to measure the AIP velocity field. The flow was seeded with di-Ethyl-Hexyl Sebacate (DEHS) particles produced by a Laskin nozzle generator with diameter of approximately $1 \mu\text{m}$. A laser light from a pulsed Nd:YAG illuminated the measurement plane. Two high-speed CMOS cameras, in stereoscopic optical arrangement were used to image the flow. Their sensor resolution was of $800 \times 1280 \text{ px}^2$. The measurements were acquired at a velocity field frequency of 8 kHz. A total number of 20,000 snapshots were acquired per dataset. This was previously found sufficient for statistical convergence of the results (see Gil-Prieto et al. [4]). A direct image cross-correlation method was applied, with a final search window of $32 \times 32 \text{ px}^2$ and 50% overlap. That yielded roughly 1,800 3-dimensional velocity vectors across the AIP whose spatial resolution was 2.2 mm^2 in both directions. The measurement uncertainty on the 3- dimensional velocity was found to be within 3% of the time and area averaged streamwise velocity at the AIP, using the method by Raffel et al. [25].

For the CFD simulations the UCNS3D solver was used. UCNS3D is a high-order CFD software framework extensively validated against experimental and computational results for subsonic/transonic/supersonic/hypersonic laminar, transitional, and fully turbulent flows [26]-[28]. A detailed description of the computational framework, numerical methods and models used can be found in the reference paper for UCNS3D [24]. For this study UCNS3D is deployed with Godunov-type method for the convective terms of the Reynolds-Averaged Navier-Stokes (RANS) equations, more specifically a 3rd-order MUSCL scheme using the MOGE limiter [24], with unsplit multidimensional reconstruction of the conserved variables is used with an HLLC Riemann solver as described in [26]. A key-ingredient of the approach is the use of the simple low-Mach number treatment of Simmonds et al., [30] which reduces the dissipation of multidimensional reconstruction at low-Mach number flow regions (close to the boundary layer) in the presence of hexahedral cells. The solution is advanced in time with a 2nd-order dual-time stepping method, that uses an approximate Jacobian LU-SGS technique for accelerating the convergence to the pseudo-state problem and local time stepping as described in [24]. The RANS equations are closed with the Spalart-Allmaras turbulence model, which uses the same spatial discretization as the mean flow variables.

The simulations for the current work were set up by applying an inlet velocity boundary condition which imposes the defined Mach number 0.27 and a non-reflecting gauge pressure outlet condition. The latter is required to damp out the pressure waves created in the fluid domain by the inlet velocity condition, due to the mildly compressible nature

of the solver. To achieve a fully established unsteady solution, a total simulation time of 0.66 sec was set which corresponds to approximately x85 through-flow (convective) times calculated based on the mean axial velocity at the reference plane and the length of the S-duct mean line ($t_{conv}=0.0078$ sec). Only the last 60 convective times were considered for the post-processing in order to avoid the initial transient part of the simulation from the steady to the established unsteady solution. A time-step of $1.5e-5$ sec was used. The three-component velocity vector, static pressure and static temperature were extracted from the S-duct's exit plane probes every one time-step which resulted in an output signal frequency at each probe of approximately 44 kHz. This CFD signal was subsequently under-sampled in time prior to any further post-processing to match the temporal frequency of the experimental velocities (8kHz). The reader should take note of the fact that the array of probes at the CFD simulation was placed at the S-duct's exit plane, which yields a discrepancy in its streamwise location with respect to the TR-PIV data which was acquired $0.4D_{out}$ downstream of the exit plane.

The processing of the time dependent data generated by both the CFD simulation, and the TR-PIV experiment was processed using the newly developed MIDAS (Modern Intake Distortion Analysis System) software platform. MIDAS is a Cranfield developed Python library of codes that was bespoke designed for the characterization of non-uniform flows at an Aerodynamic Interface cross-flow plane. It was developed as part of EU funded programmes. The system enables a range of time dependent calculations of the cross-flow quantities with the primary aim to characterize dynamic flow distortions of total pressure or flow angularity. Further capabilities include derivation of unsteady distortion properties and the calculation of unsteady orthogonal modes via a range of methods. One of the main features of MIDAS is that the data is stored in Hierarchical Data Format (HDF5), which is an open-source file format that permits to store large amounts of data very efficiently. The minimum number of variables required by the code to perform the analysis are the coordinates (x and y) and the three velocity components (u, v, w) at points on a given cross-flow plane between the highlight plane of the intake and the fan face.

III. Results and Discussion

The computed and measured time-averaged, normalized out-of-plane velocities and swirl angles across the AIP are shown in Figure 2. In these contours, w is used to indicate the velocity along the z-axis which is the out-of-plane vector. Swirl angle (α) is defined as the angle between the tangential and the out-of-plane velocity vectors at each point of the AIP ($\alpha = \arctan(V_t/w)$). The blank region between the boundary of the AIP and the experimental flow contours (Figure 2c, d) indicates the region where TR-PIV data showed uncertainty higher than 10% in the out-of-plane velocity and is not included in the analysis. The mean out-of-plane velocity distribution is characterized by a low velocity zone located centrally at the AIP and extending towards the lower and central part of it as previously shown by Zachos et al. [3] and Gil-Prieto et al. [4]. This low velocity zone is primarily the result of a separation region that is initiated within the first bend of the diffuser and subsequently influences the flow angularity observed across the measurement plane (Figure 1). The HODDES computed velocity and swirl angle distributions (Figure 2a, b) show a notably wider range when compared with the PIV measurements (Figure 2c, d). The HODDES flow distributions indicate 50% lower velocities at the bottom and central part of the AIP than the experimental results with also notably higher velocities across the rest of the AIP, suggesting that the mass flow distribution across the exit plane of the duct is differently predicted compared to the TR-PIV experiments. This is reflected on the variation of the swirl angle which for the HODDES cases was found more than 80% higher than in the experimental ones, indicating swirl angle values across a range of approximately $\pm 24^\circ$. A possible route for this discrepancy may be related to the prediction of the flow separation that occurs within the S-duct and which the HODDES method probably over-predicts terms of size and extent. Overprediction of the flow unsteadiness by about 80% is also shown in the HODDES results when compared to the TR-PIV measured data (Figure 3). Flow unsteadiness is herein expressed as the normalized standard deviation of the out of plane velocity and standard deviation of the swirl angle. Nevertheless, the broader distribution of the normalized out of plane velocity and swirl angle shows a zone of highly unsteady content across the central and bottom part of the AIP, whereas these fluctuations exhibit lower levels across the upper region of the plane. In particular, The HODDES predictions indicate a zone on notably low unsteadiness at the top part of the plane (Figure 3a), which is not shown by the test data. This is potentially due to the streamwise discrepancy between the CFD and experimental cross-flow planes that was described earlier. By interrogating the CFD flow field further downstream (Figure 4), it was seen that indeed this low unsteadiness zone shown at the top of the exit plane is related to a shear layer that develops in this region and becomes highly unsteady more downstream and nearer the streamwise location of the TR-PIV plane ($0.4D_{out}$). The time-average and unsteady flow distributions suggest that the deployed HODDES

model is broadly able to predict the AIP flow topologies, but it is expected to generate more unsteady temporal histories of distortion near the exit plane of the S-duct. These are expected to fluctuate around an also substantially higher mean value than the TR-PIV observed results, yielding a dynamic distortion population characterized by notably more extreme events whose magnitude is investigated in a subsequent section.

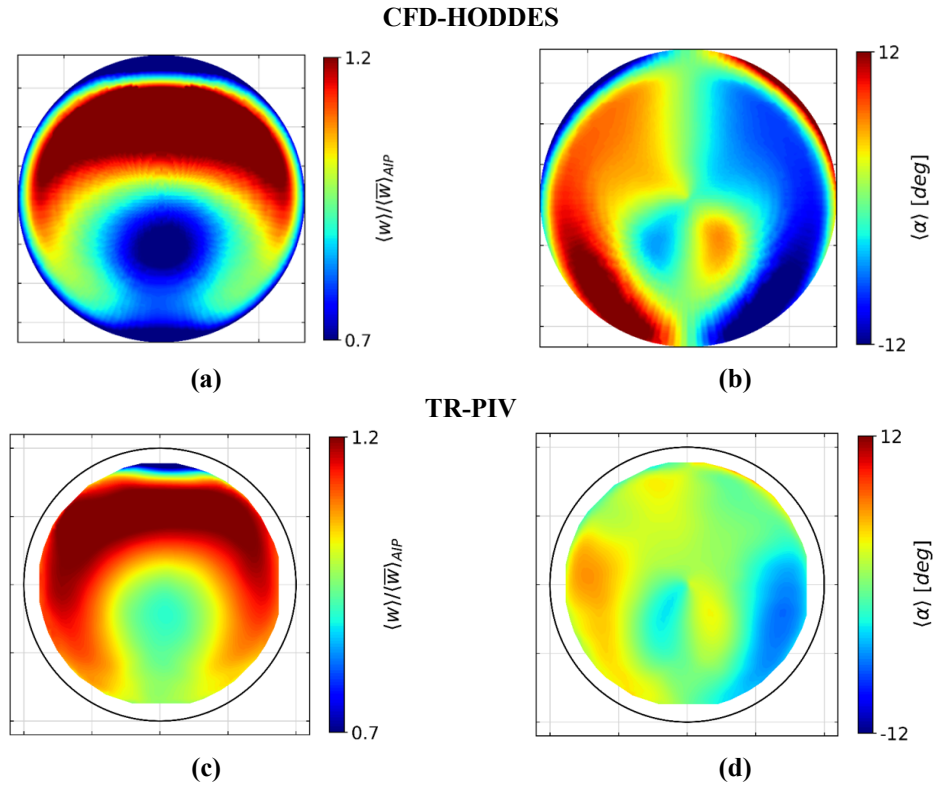
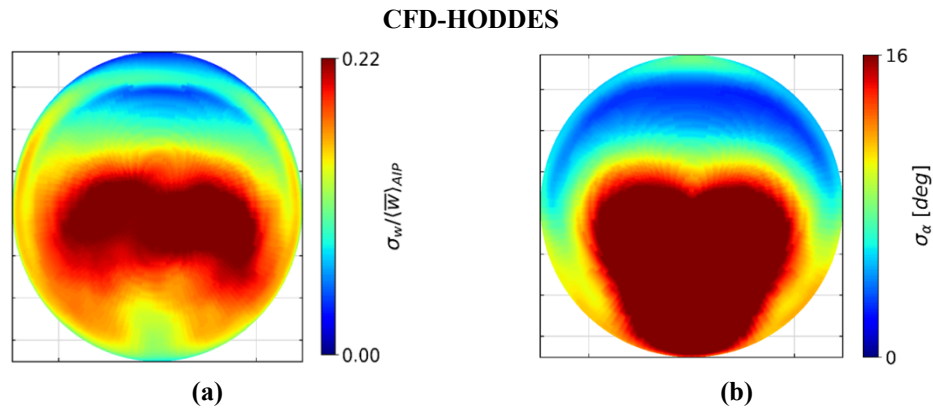


Figure 2 Computed (top) and measured (bottom) time-averaged out of plane velocity and swirl angle profiles for the S-shaped diffuser at $M_{ref}=0.27$.



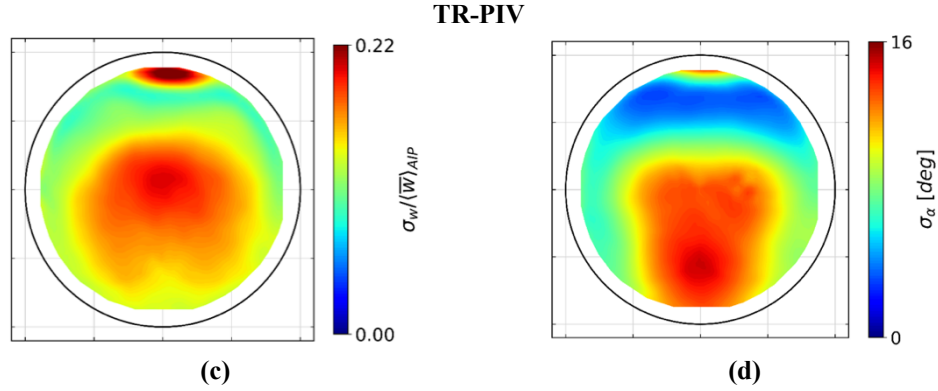


Figure 3 Computed (top) and measured (botttom) unsteady out of plane velocity and swirl angle profiles for the S-shaped diffuser at $M_{ref}=0.27$.

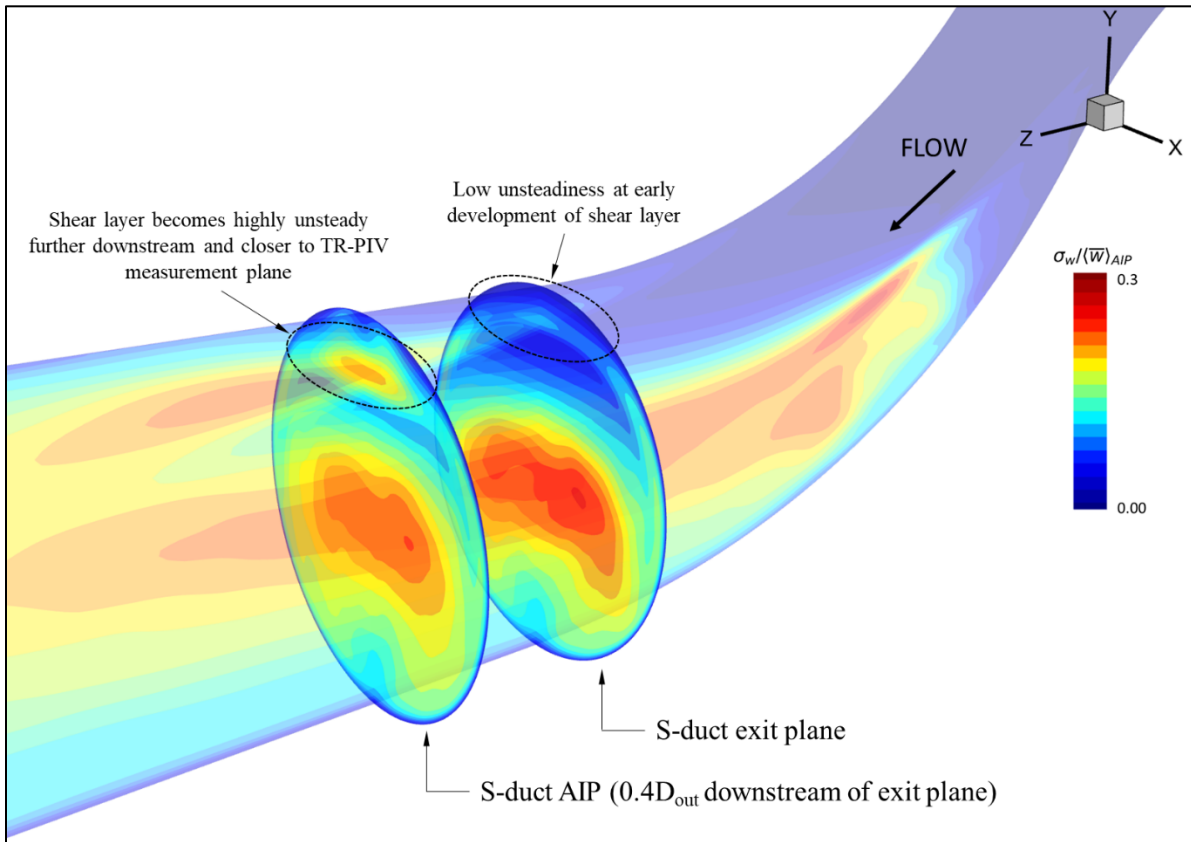
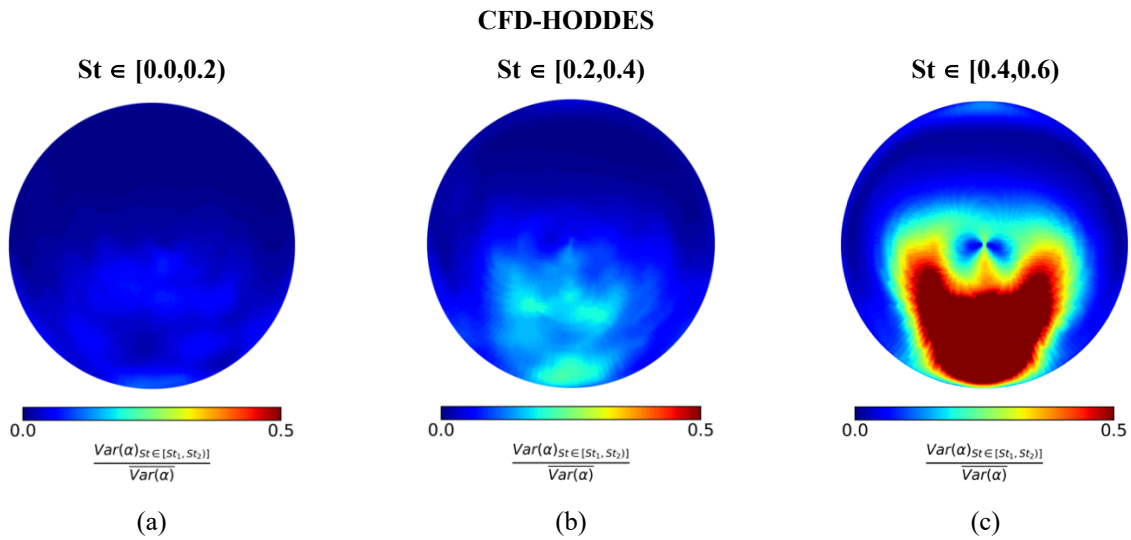


Figure 4 Variation of the HODDES predicted unsteadiness between the duct's exit plane where CFD probes where place and the AIP at $0.4D_{out}$ where the TR-PIV data was acquired.

It is of interest to investigate the frequency content of the unsteady flow was previously linked to the operability margin of the propulsion system (see [8]-[10]). Hathaway et al. [29] previously indicated a critical frequency range within which a fan rotor is likely to result in notable penalties to its surge margin. For a typical transonic fan rotor this range was approximately identified as $St=0.9-5.4$ ([29] [30]). The lower bound was obtained assuming the first engine order frequency, while the upper bound considered the time needed for a blade of a typical transonic fan rotor with diameter in the order of D_{out} to cover a sector of 60° across the AIP [20]. Gil-Prieto et al. [20] showed a spectral analysis of each velocity component using TR-PIV data. This enabled the cross-correlation of the spectral content with the critical frequency range to determine the likelihood of a potential fan operability penalty.

The power spectrum (PS) of the unsteady velocity signals obtained by the HODDES and TR-PIV was evaluated at each point of the S-duct AIP at $M_{ref}=0.27$ for the range of inlet flow profiles. The analysis was performed using Welch's average periodogram method [31]. To perform the band discretization and prevent frequency leakage, a Hann window was applied. The time average value of each velocity component was subtracted prior to the FFT to reduce the uncertainty of the transformation. The signal was finally filtered in frequency bands of $St = 0.2$ wide. The results of the area average flow variance for each velocity component were non-dimensionalized with the area average, mean turbulent kinetic energy content across the whole AIP. The St number resolution across each band was approximately $\Delta St=0.025$. The swirl angle variance distributions across each spectral band is non-dimensionalized by the area averaged swirl angle variance across the whole spectrum $Var(\alpha)_{St \in [St_1, St_2]} / \overline{Var(\alpha)}$ (Figure 5 HODDES, Figure 6 TR-PIV).

The HODDES showed the dominant unsteady swirl angle fluctuations within the $St=0.4-0.8$ bands (Figure 5c and i) located at the lower part of the AIP. The unsteady zone in the TR-PIV dataset (Figure 6c) was also located the lower and central part of the AIP extending across the same regime where the low velocity zone was previously identified. In this case, however, the unsteady activity was found to be limited within a single St band between $0.4 - 0.6$ which is a notable variation from the HODDES finding. The spectral content across the rest of the bands is notably lower than the content of the $St=0.4-0.6$ band and this observation remains valid for both the HODDES as well as the TR-PIV datasets. The topology of the spectral contributions is also in agreement between the two methods indicating high swirl angle fluctuations in the central part of the domain extending across the left and the right side of the AIP's vertical symmetry axis. This observations about the swirl angle unsteady fluctuations are aligned with the justification of the swirl switching mechanism previously demonstrated by Gil-Prieto et al. [20] where this mechanism was identified to occur within the same spectral band of $St=0.4-0.6$ of the unsteady in-plane and out-of-plane velocity components measured with TR-PIV for the same S-duct geometry at $M_{ref}=0.27$. The impact of the unsteady content distribution on the stability of a low-pressure fan system remains an open question. According to the authors' knowledge, this is an aspect that was never previous addressed in any past work, but it is of vital importance and can influence the design approach of a closely coupled fan-intake system.



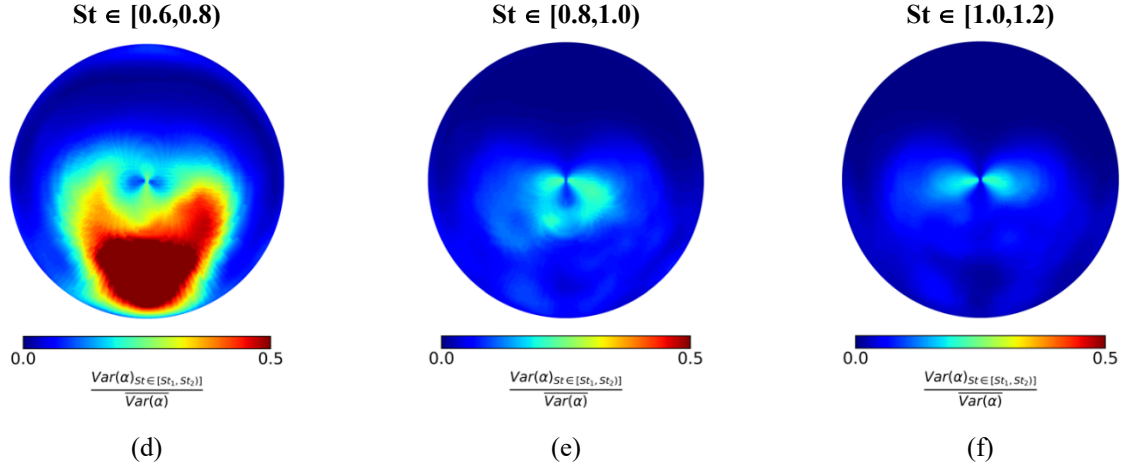


Figure 5 Spectral distribution of swirl angle fluctuations obtained with HODDES for the S-duct with $M_{ref}=0.27$.

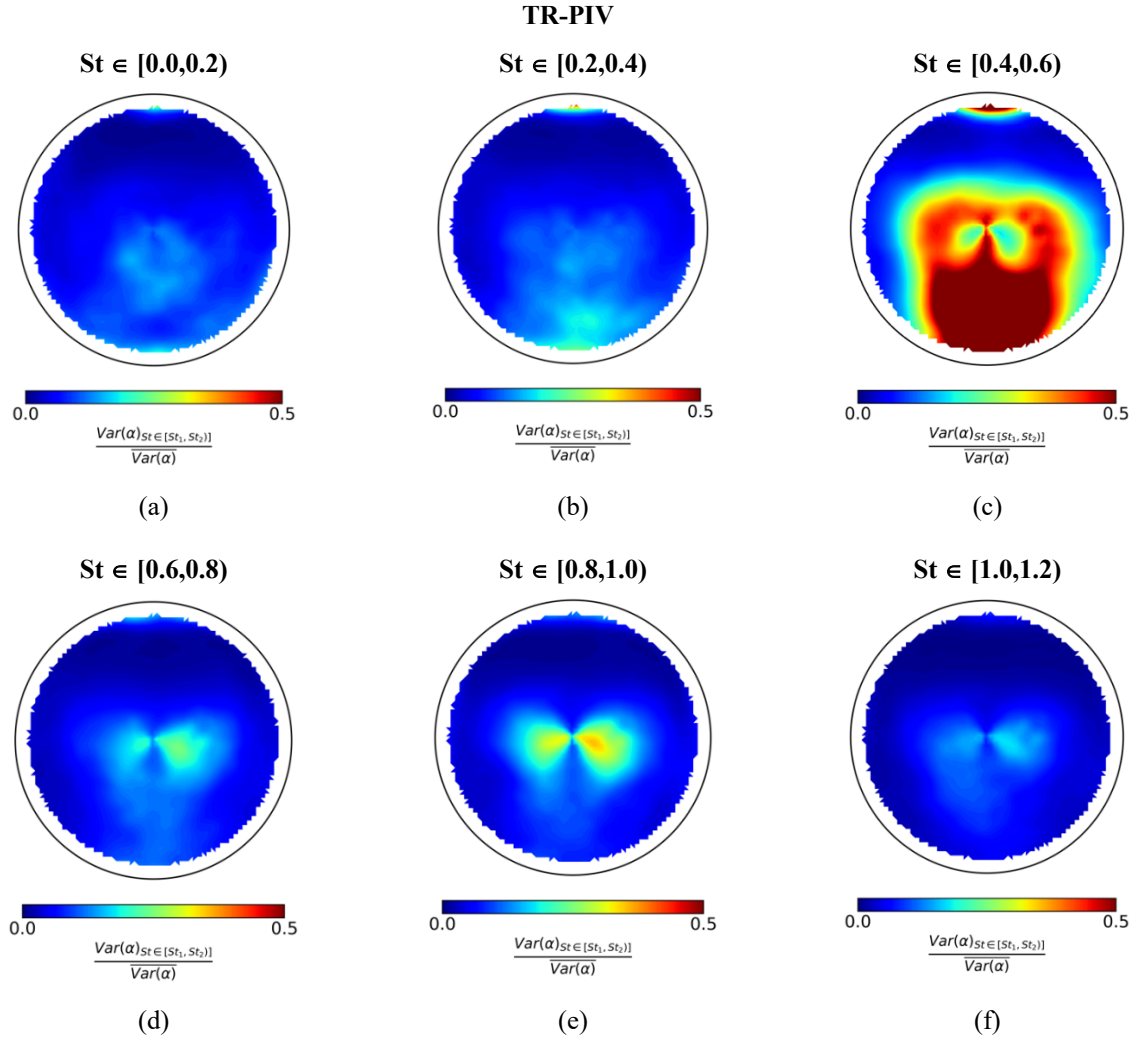


Figure 6 Spectral distribution of swirl angle fluctuations obtained with TR-PIV for the S-duct with $M_{ref}=0.27$.

To quantify the unsteady distortion levels and facilitate fan-intake coupling exercises, flow distortion descriptors were previously introduced by the Society of Automotive Engineers SAE [6]. These are defined based on a discretization of the AIP into radial rings. The basis for these definitions is the 2-per-rev swirl pattern shown in Figure 7. Swirl angle is considered to be positive based on the AIP viewed from downstream and a counter-clockwise direction. A range of swirl descriptors are defined based on sector swirl and extents that quantify the nature and strength of the swirl distortion. The *Swirl Intensity* (SI, Eq. 1), *Swirl Directivity* (SD, Eq. 2) and the *Swirl Pairs* (SP, Eq. 3) represent the magnitude of the absolute swirl angle, the overall spinning direction, and the number of paired swirl patterns at the AIP ring i , respectively. In this work, swirl descriptors were calculated at five equal area rings to align the layout with SAE compliant arrangements commonly used for industrial distortion measurements ([6]) for both HODDES and TR-PIV data. To do so, both datasets were interpolated considering 72 equi-spaced circumferential points for each ring which yields a circumferential spacing of 5 deg.

The instantaneous flow fields predicted by the UCNS3d HODDES method were used for the calculation of instantaneous swirl descriptor values at a total of five radial rings across the AIP. The radial ring at $r/R=0.837$ is only reported here. The descriptors are reported in pairs to enable a more representative illustration of the distorted flow profiles at the AIP at each time instance (Figure 8) at a prescribed radial position. The relative occurrence frequency of these events was also included in these maps as an additional parameter. Joint Probability Density Function maps (j-PDF) were then generated using both the CFD and test data. To evaluate the j-PDF, the range of each descriptor was discretized in 60 equi-spaced partitions which yielded a resolution of approximately 0.03 for SP and SD. Integration of the PDF over the desired part of the range (Eq. 4) reflects the probability to identify the distorted pattern within a given region of the SP-SD envelope. Examples of such representation were shown previously by Zachos et al. in [3] and Gil-Prieto et al. [4] [5] using PIV results from S-shaped diffuser experiments. The distortion descriptor maps enable the assessment of the dynamic behavior of the swirl topologies, which are known to be significantly different from the time-averaged representation of the flow where two vortical patterns are symmetrically located at the lower part of the AIP.

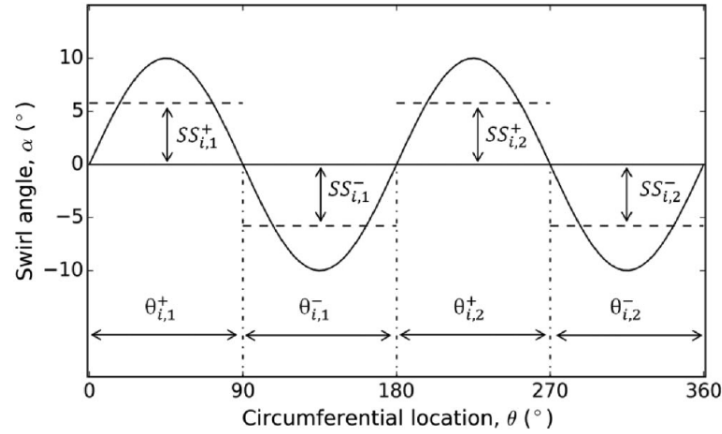


Figure 7 Example of 2-per-rev swirl pattern [6].

$$SI(i) = \frac{\sum_{k=1}^m SS_{i,k}^+ \cdot \theta_{i,k}^+ + \sum_{k=1}^m |SS_{i,k}^-| \cdot \theta_{i,k}^-}{360} \quad (1)$$

$$SD(i) = \frac{\sum_{k=1}^m SS_{i,k}^+ \cdot \theta_{i,k}^+ + \sum_{k=1}^m SS_{i,k}^- \cdot \theta_{i,k}^-}{\sum_{k=1}^m SS_{i,k}^+ \cdot \theta_{i,k}^+ + \sum_{k=1}^m |SS_{i,k}^-| \cdot \theta_{i,k}^-} \quad (2)$$

$$SP(i) = \frac{\sum_{k=1}^m SS_{i,k}^+ \cdot \theta_{i,k}^+ + \sum_{k=1}^m |SS_{i,k}^-| \cdot \theta_{i,k}^-}{2 \cdot \text{Max}\{SS_{i,k}^+ \cdot \theta_{i,k}^+, |SS_{i,k}^-| \cdot \theta_{i,k}^-\}_{k=1,\dots,m}} \quad (3)$$

$$P(SD_A \leq SD < SD_B, SP_A \leq SP < SP_B) = \int_{SP_A}^{SP_B} \int_{SD_A}^{SD_B} PDF \, dSD \, dSP \quad (4)$$

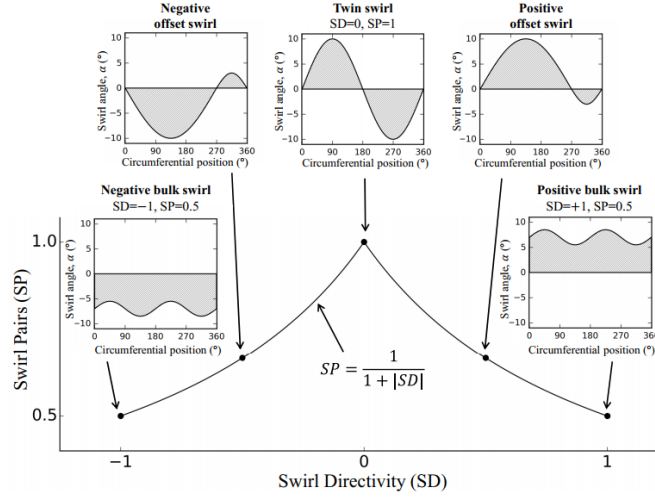


Figure 8 Bulk-to-twin swirl switching path along one revolution [17].

The analysis of the current results indicates that the HODDES dataset includes instantaneous distortion events with notably less extreme values than the ones observed at the TR-PIV experiment. In particular, for example, the TR-PIV population shows a large number of individuals with two or more swirl pairs co-existing at the AIP, whereas this is not the case for the HODDES results where one or 1.5 pairs were observed for only a few cases (Figure 9a and d) with notably lower dispersion than the one showed by the experimental data. In addition, the entire population of the HODDES dataset indicates slightly higher levels of SI of circa 14° at $r/R=0.837$ (towards the tip region of a notional fan), while the TR-PIV produced a range between 4° - 13° with most of them between 5° - 8° , which is a significant variation from the calculated ones. (Figure 9b and e). These observations are linked with the earlier points about the higher unsteadiness observed at the TR-PIV dataset that was mainly attributed to the discrepancy between the CFD and TR-PIV streamwise positions (Figure 4) which introduced the influence of the shear layer unsteadiness on the dynamic distortion descriptor populations of Figure 9. This is an area where more effort will be needed in the future to better understand the stream wise variation of the flow downstream of the duct's exit plane and the various pertinent modelling aspects.

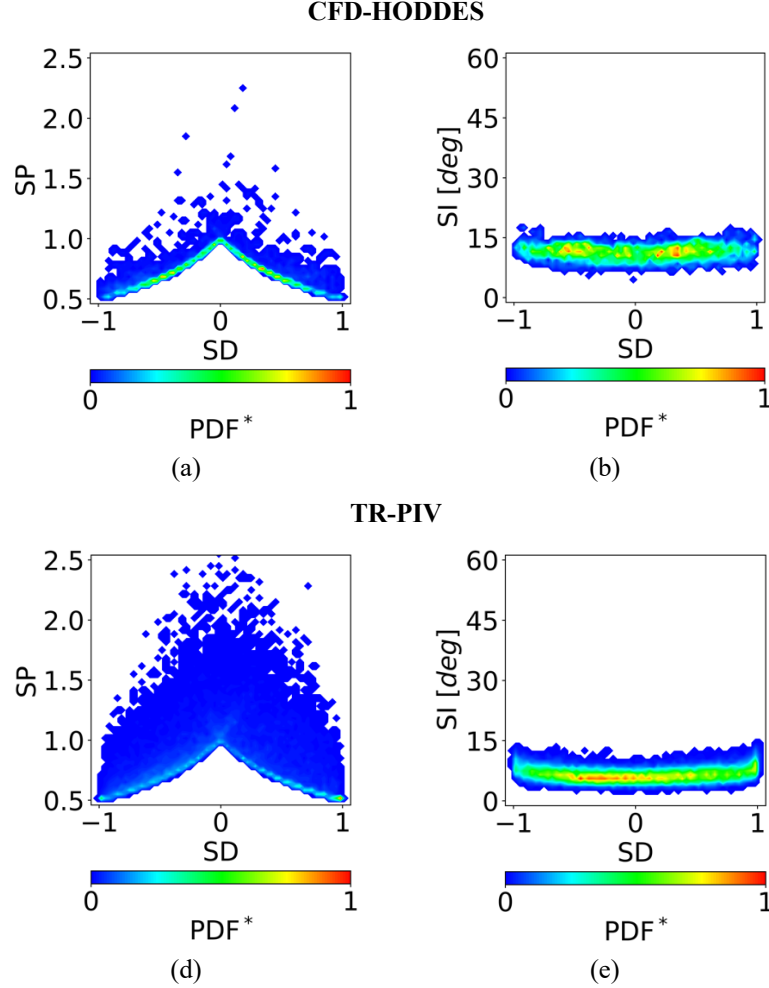


Figure 9 HODDES and TR-PIV distortion probability maps at $r/R=0.837$ (tip) at $M_{ref}=0.27$.

IV. Conclusions

An in-house CFD solver previously developed at Cranfield University was used to calculate the dynamic flow distortion characteristics at the exit of a convoluted, S-shaped diffuser very commonly used in closely coupled aircraft-engine systems for current and novel architectures. The aim of the work was to understand the predictive capability of this new computational tool, prior to its deployment for the simulation of a fully coupled fan-intake system for the evaluation of fan stability levels in presence of dynamic distortion. The current analysis showed the UCNS3d HODDES model applied herein generates notably more unsteady flows than the ones observed during the TR-PIV experiments. The computed flows are characterized by 40% higher velocity levels across the AIP with unsteady fluctuations approximately 60-80% higher than the ones observed during the experiment. This is also reflected in the swirl angle and swirl distortion descriptor variations whose calculation rely on the predicted unsteady velocities across the plane. The HODDES scheme provides a high-order low-dissipation alternative to traditional DDES employed with 2nd-order methods, and therefore possesses favorable modelling characteristics in the LES regions of the flow. As such, further calibration might be required to ensure that the RANS region does not overwhelm the LES regions with the advection of large-quantities of turbulent viscosity in future applications. In subsequent steps of the current work UCNS3d unsteady predictions will be used to convert the unsteady swirl angle distributions into fan-relevant metrics such as unsteady incidence angle profiles as shown in [32]. To do, so a notional fan rotor geometry will be assumed at a suitable rotational installed at the exit of the diffuser. The numerical results will be validated against TR-PIV

datasets off an experiment conducted with a fan in place. The outcome of this future work is expected to quantify the variations in unsteady distortion predictions produced by the method shown in [32] and, as a result, its applicability for fan-intake integration studies during the early and/or conceptual stage of a new system's design.

This work presented in this paper was partially conducted under project SINATRA which received funding from the CLEAN SKY 2 Joint Undertaking (JU) under Grant Agreement no. 886521. The JU receives support from the European Union's Horizon 2020 research and innovation programme and the CLEAN SKY 2 JU members other than the Union.

References

- [1] Kawai, R.T., Friedman, D.M., and Serrano L., "Blended Wing Body (BWB) Boundary Layer Ingestion (BLI) Inlet Configuration and System Studies," NASA Technical Report CR-2006-214534, 2006.
- [2] Florea, R.V., Matalanis, C., Hardin, L.W., Stucky, M., and Shabbir, A., "Parametric Analysis and Design for Embedded Engine Inlets," *Journal of Propulsion and Power*, Vol. 31, No. 3, 2015, pp. 843-850. DOI: 10.2514/1.B34804
- [3] Zachos, P.K., MacManus, D.G., Gil-Prieto, D., and Chiereghin, N., "Flow Distortion Measurements in Convoluted Aeroengine Intakes," *AIAA Journal*, Vol. 54, No. 9, 2016, pp. 2819-2832. DOI: 10.2514/1.J054904
- [4] Gil-Prieto, D., MacManus, D.G., Zachos, P.K., Tanguy, G., and Menzies, K.R., "Convoluted Intake Distortion Measurements Using Stereo Particle Image Velocimetry," *AIAA Journal*, Vol. 55, No. 6, 2017, pp. 1878-1892. DOI: 10.2514/1.J055467
- [5] Gil-Prieto, D., MacManus, D.G., Zachos, P.K., Tanguy, G., and Wilson, F., Chiereghin, N., "Delayed Detached-Eddy Simulation and Particle Image Velocimetry Investigation of S-Duct Flow Distortion," *AIAA Journal*, Vol. 55, No. 6, 2017, pp. 1893-1908. DOI: 10.2514/1.J055468
- [6] Society of Automotive Engineers, "A Methodology for Assessing Inlet Swirl Distortion," SAE Aerospace Information Report 5686, 2007.
- [7] Kidman D. S., Reagan, P. V., and Malloy, D. J., "Comparison of Inlet Compatibility Results from Subscale Wind Tunnel and Full-Scale Flight Tests of the F/A-22 Aircraft with the F119-PW-100 Engine," *Proceedings of the 17th Symposium on Air Breathing Engines, International Soc. of Air Breathing Engines*, ISABE-2005-1169, 2005.
- [8] Wenzel, L.M., and Blaha, R.J., "Analysis of Dynamic Inlet Distortion Applied to a Parallel Compressor Model," NASA TM X-3522, 1977.
- [9] Rademakers, R.P.M., Bindl, S., and Niehuis, R., "Effects of Flow Distortions as they Occur in S-Duct Inlets on the Performance and Stability of a Jet Engine," *Journal of Eng. for Gas Turbines and Power*, Vol. 138, No. 2, 2015. DOI:10.1115/1.4031305
- [10] Cousins, W.T., "History, Philosophy, Physics and Future Directions of Aircraft Propulsion System / Inlet Integration," *Proceedings of ASME Turbo Expo 2004: Power for Land, Sea, and Air*, Vol. 2, GT2004-54210, 2004, pp. 305-320. DOI: 10.1115/GT2004-54210
- [11] Bowditch, D.N., and Coltrin, R.E., "A Survey of Inlet/Engine Distortion Compatibility," NASA TM-83421, 1983.
- [12] Wellborn, S.R., Reichert, B.A., and Okiishi, T.H., "Study of the Compressible Flow in a Diffusing S-Duct," *Journal of Propulsion and Power*, Vol. 10, No. 5, 1994, pp. 668-675. DOI: 10.2514/3.23778
- [13] Delot, A.-L., Garnier, E., and Pagan, D., "Flow Control in a High-Offset Subsonic Air Intake," *47th AIAA/ASME/SAE/ASEE Joint Propulsion Conference & Exhibit*, AIAA 2011-5569, San Diego, California, 2011. DOI: 10.2514/6.2011-5569
- [14] Delot A.-L., and Scharnhorst, R.K., "A Comparison of Several CFD Codes with Experimental Data in a Diffusing S-Duct," *49th AIAA/ASME/SAE/ASEE Joint Propulsion Conference & Exhibit*, AIAA 2013-3796, San Jose, California, 2013. DOI: 10.2514/6.2013-3796
- [15] Delot, A.-L., Berens, T.M., Tormalm, M.H., Sätterskog, M., and Ceresola, N., "DES Computations for a Subsonic UAV Configuration with a Highly Integrated S-Shaped Intake Duct," *52nd Aerospace Sciences Meeting*, AIAA 2014-0723, National Harbor, Maryland, 2014, DOI: 10.2514/6.2014-0723
- [16] Garnier, E., "Flow Control by Pulsed Jet in a Curved S-Duct: A Spectral Analysis," *AIAA Journal*, Vol. 53, No. 10, 2015, pp. 2813-2827. DOI: 10.2514/1.J053422
- [17] Giuliani, J.E., and Chen, J.-P., "Fan Response to Boundary-Layer Ingesting Inlet Distortions," *AIAA Journal*, Vol. 54, No. 10, 2016, pp. 3232-3243. DOI: 10.2514/1.J054762

- [18] McLelland, G., MacManus, D. G., Zachos, P. K., Gil-Prieto, D., and Migliorini, M., "Influence of Upstream Total Pressure Profiles on S-Duct Intake Flow Distortion," *Journal of Propulsion and Power*, Vol. 36, No. 3, 2020, pp. 0–0. <https://doi.org/10.2514/1.b37554>
- [19] Migliorini, M., Zachos, P. K., MacManus, D. G., and Haladuda, P., "S-Duct Flow Distortion with Non-Uniform Inlet Conditions," *Proceedings of the Institution of Mechanical Engineers, Part G: Journal of Aerospace Engineering*, 2022, p. 095441002211016. <https://doi.org/10.1177/09544100221101669>
- [20] Gil-Prieto, D., Zachos, P.K., MacManus, D.G., and McLelland, G., "Unsteady Characteristics of S-duct Intake Flow Distortion," *Aerospace Science and Technology*, Vol 84, 2018, pp. 938-952. DOI: <https://doi.org/10.1016/j.ast.2018.10.020>
- [21] MacManus, D.G., Chiereghin, N., Gil-Prieto, D., and Zachos, P.K., "Complex Aeroengine Intake Ducts and Dynamic Distortion," *ALAA Journal*, Vol. 55, No. 7, 2017, pp. 2395-2409. DOI: 10.2514/1.J054905
- [22] Kalpakli-Vester, A., Örlü, R., and Alfredsson, P.H., "POD Analysis of the Turbulent Flow Downstream a Mild and Sharp Bend," *Experiments in Fluids*, Vol. 56, No. 3, 2015. DOI: 10.1007/s00348-015-1926-6
- [23] Dean, W.R., "Note on the Motion of Fluid in a Curved Pipe," *The London, Edinburgh, and Dublin Philosophical Magazine and Journal of Science*, Vol. 4, No. 20, 1927, pp. 208-223. DOI: 10.1080/14786440708564324
- [24] Antoniadis, A.F., Drikakis, D., Farmakis, P., Fu, L., Kokkinakis, I. W., Nogueira, X., Silva, P.A.S.F., Skote, M., Titarev, V., Tsoutsanis, P., "UCNS3D: An Open-Source High-Order Finite-Volume Unstructured CFD Solver", *Computer Physics Communications*. Vol 279, 108453, (2022), doi:10.1016/j.cpc.2022.108453
- [25] Raffel, M., Willert, C., Wereley, S., and Kompenhans, J., *Particle Image Velocimetry: A Practical Guide*, 2nd ed., Springer-Verlag, Berlin, 2007, Chap. 5, DOI: 10.1007/978-3-540-72308-0
- [26] Silva, P. A.S.F., Antoniadis, A. F., Tsoutsanis, P. "A Simple Multiple Reference Frame for High-Order Solution of Hovering Rotors with and without Ground Effect", *Aerospace Science and Technology*, Vol 111, 106518, (2021), doi:10.1016/j.ast.2021.106518
- [27] Antoniadis, A. F., Tsoutsanis, P., Drikakis, D., "Assessment of high-order finite volume methods on unstructured meshes for RANS solutions of aeronautical configurations", *Computer and Fluids*, Vol 146, pp. 86-104, (2017), doi:10.1016/j.compfluid.2017.01.002
- [28] Tsoutsanis, P., Antoniadis, A. F., Drikakis, D., "WENO Schemes on Arbitrary Unstructured Meshes for Laminar, Transitional and Turbulent Flows", *Journal of Computational Physics*, Vol 256, pp. 254-276, (2014), doi:10.1016/j.jcp.2013.09.002
- [29] Hathaway, M. D., Okiishi, T. H., Suder, K. L., Strazisar, A. J., and Adamczyk, J. J. "Measurements of the Unsteady Flow Field Within the Stator Row of a Transonic Axial-Flow Fan: II — Results and Discussion," *Proceedings of the ASME 1987 International Gas Turbine Conference and Exhibition. Volume 1: Turbomachinery*, Anaheim, California, USA, 1987. DOI: <https://doi.org/10.1115/87-GT-227>
- [30] Paul, D.L., and Younghans, J.L., "Inlets and Inlet Engine Integration. The Aerothermodynamics of Aircraft Gas Turbine Engines", edited by Oates, G. C., Report AFAPL TR 78-52, University of Washington Seattle, 1978.
- [31] Welch, P.D., "The Use of Fast Fourier Transform for the Estimation of Power Spectra: A Method Based on Time Averaging Over Short," *Modified Periodograms. IEEE Transactions on Audio and Electroacoustics*, Vol. 15, No. 2, 1967, pp. 70-73. DOI: 10.1109/TAU.1967.1161901
- [32] Migliorini, M., Zachos, P. K., and MacManus, D. G., "Novel Method for Evaluating Intake Unsteady Flow Distortion," *Journal of Propulsion and Power*, 2021, pp. 1–13. <https://doi.org/10.2514/1.b38127>

2024-01-04

Dynamic swirl distortion characteristics in S-shaped diffusers using UCNS3D and time-resolved, stereo PIV methods

Piovesan, Tommaso

AIAA

Piovesan T, Migliorini M, Zachos PK, Tsoutsanis P. (2024) Dynamic swirl distortion characteristics in S-shaped diffusers using UCNS3D and time-resolved, stereo PIV methods. In: AIAA SCITECH 2024 Forum, 8-12 January 2024, Orlando, USA. Paper number AIAA 2024-1196 <https://doi.org/10.2514/6.2024-1196>

Downloaded from Cranfield Library Services E-Repository